The Journal of Chemical Physics

RESEARCH ARTICLE | JUNE 15 1991

High resolution laser spectroscopy up to the dissociation limit of the NaK *B* $^1\Pi$ state, and predissociation near the dissociation limit

Shunji Kasahara; Masaaki Baba; Hajime Katô

Check for updates

J. Chem. Phys. 94, 7713–7720 (1991)
https://doi.org/10.1063/1.460157

View Online
Export Citation
CrossMark

Articles You May Be Interested In

Near-infrared spectra of the NaK molecule
J. Chem. Phys. (November 1985)

Ultrafast multiphoton ionization dynamics and control of NaK molecules
J. Chem. Phys. (December 1998)

Collisional transfer of population and orientation in NaK
J. Chem. Phys. (May 2011)

Downloaded from http://pubs.aip.org/aip/jcp/article-pdf/94/12/7713/9732731/7713_1_online.pdf

AIP Publishing

The Journal of Chemical Physics

Special Topic: Adhesion and Friction

Submit Today!

AIP Publishing

High resolution laser spectroscopy up to the dissociation limit of the NaK $B\,^1\Pi$ state, and predissociation near the dissociation limit

Shunji Kasahara, Masaaki Baba,[a] and Hajime Katô
Department of Chemistry, Faculty of Science, Kobe University, Nada-ku, Kobe 657, Japan

(Received 31 December 1990; accepted 4 March 1991)

Doppler-free high resolution spectrum of the $B\,^1\Pi(v',J')$–$X\,^1\Sigma^+(v'',J'')$ transitions of $^{23}Na^{39}K$ was measured by the optical–optical double resonance (OODR) polarization spectroscopy. The transition lines up to the $v' = 43$ level, which was estimated to be 1.8 cm^{-1} below the dissociation limit, were observed. The potential energy curve for internuclear distance from 3.25 to 15.6 Å was calculated by the RKR method, and the inverse-power coefficient was determined by analyzing the long-range RKR turning points. The $B\,^1\Pi$ state dissociates to $Na(3s^2S_{1/2}) + K(4p^2P_{3/2})$ atoms without a potential hill near the dissociation limit. The dissociation energy was determined to be 1324.3 ± 0.3 cm^{-1} from the LeRoy–Bernstein plots. Remarkable line broadenings were observed for transitions higher than the dissociation energy to $Na(3s^2S_{1/2}) + K(4p^2P_{1/2})$ atoms. This is identified as originating from the predissociation to $Na(3s^2S_{1/2}) + K(4p^2P_{1/2})$ atoms. The predissociation is shown to be caused by a spin–orbit interaction between the $B\,^1\Pi$ and $(2)^3\Sigma^+$ states, and the potential curves are expected to cross around the inner turning point of the $B\,^1\Pi(v' = 34)$ level.

I. INTRODUCTION

The $B\,^1\Pi$ state of the alkali metal diatomic molecules is correlated with separated atoms in the $^2S_{1/2}$ and $^2P_{3/2}$ states. The $B\,^1\Pi_u$ state of homonuclear molecules has a potential barrier caused by a repulsive long-range resonant dipole interaction.[1] Chawla *et al.*[2] determined the shape of the Na_2 $B\,^1\Pi_u$ state potential barrier by measuring the rotation–vibration line energies and linewidths of the quasibound levels using the technique of modulated gain spectroscopy. Heinze *et al.*[3] determined the K_2 $B\,^1\Pi_u$ state potential barrier. There is no resonant dipole interaction in heteronuclear molecules, and the NaK $B\,^1\Pi$ state is expected to dissociate to $Na(3s^2S_{1/2}) + K(4p^2P_{3/2})$ atoms without a potential hill near the dissociation limit. In this paper, we present results which allowed us to determine the potential curve of the $^{23}Na^{39}K$ $B\,^1\Pi$ state for internuclear distance up to 15.6 Å.

Barrow *et al.*[4] obtained the molecular constants of the $B\,^1\Pi$ state of $v' = 0$–14 by analyzing the laser induced dispersed fluorescence spectra detected by a Fourier-transform spectrometer and the dye laser excitation spectra. Katô *et al.*[5] observed the $B\,^1\Pi$–$X\,^1\Sigma^+$ transition with the technique of polarization spectroscopy, and determined the molecular constants of the $B\,^1\Pi$ state of $v' = 0$–16. From the calculated Franck–Condon factors between a potential of the $B\,^1\Pi$ state extrapolated up to the dissociation limit and the RKR potential of the $X\,^1\Sigma^+$ state,[6] we noticed that high vibrational levels near the dissociation limit of the $B\,^1\Pi$ state can be excited effectively from the $X\,^1\Sigma^+(v'' = 4)$ level. However, the transition lines from $v'' = 4$ are overlapped with the strong lines from $v'' = 0$ and 1. Using the method of Doppler-free OODR polarization spectroscopy,[7–9] we could observe selectively the transitions from the $X\,^1\Sigma^+(v'' = 4)$ level to high vibrational levels close to the dissociation limit of the $B\,^1\Pi$ state. The excitation scheme is shown in Fig. 1.

We report the molecular constants of the $B\,^1\Pi$ state up to $v' = 43$, the RKR potential curve, and the inverse-power coefficient determined by analyzing the long-range RKR turning points. Remarkable line broadenings have been observed for transitions to the $B\,^1\Pi(v', J')$ levels higher than the dissociation energy to $Na(3s^2S_{1/2}) + K(4p^2P_{1/2})$ atoms. The v' dependence of the linewidth is reported in this article. We identify the line broadening as originating from the predissociation, and the mechanism is discussed.

II. EXPERIMENTAL

The experimental arrangement for a Doppler-free OODR polarization spectroscopy is shown in Fig. 2. The output of a single-mode ring dye laser 1 (Coherent CR699-21, linewidth 500 kHz, Kiton Red dye) was split into a circularly polarized strong pump beam and a linearly polarized weak probe beam. Two beams passed in opposite directions through a heat pipe. Only a small fraction of the linearly polarized probe beam, which passes a linear polarizer P1, reaches a photomultiplier PM1 (Hamamatsu R636) after passing through a crossed linear polarizer P2. If the probe beam can be absorbed by the molecules which absorb the pump beam, the probe polarization is altered from a linear to a slightly elliptical polarization. Then, the probe beam passes the crossed linear polarizer P2 and can be detected. The pump beam was modulated by a chopper (3 kHz), and the signal output was detected by a lock-in amplifier 1 (PAR model 128A). If the monochromatic laser is tuned, only the molecules with zero component of velocity along the beam direction can absorb both the pump and probe beams. The resulting signal is of Doppler-free spectral resolution, and the sensitivity is very high because the background is suppressed by the crossed polarizers. We shall call this "a nor-

[a] College of Liberal Arts and Sciences, Kyoto University, Kyoto 606, Japan.

Downloaded from http://pubs.aip.org/aip/jcp/article-pdf/94/12/7713/9732731/7713_1_online.pdf

 0021-9606/91/127713-08$03.00 © 1991 American Institute of Physics

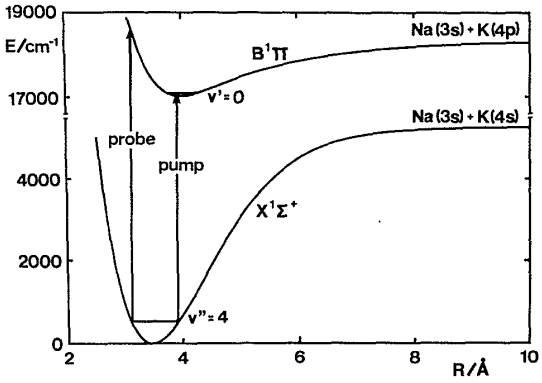

FIG. 1. A scheme of the V-type OODR polarization spectroscopy to study high vibrational levels close to the dissociation limit of the $B\,^1\Pi$ state.

mal Doppler-free polarization spectrum."[9]

A technique of a Doppler-free OODR polarization spectroscopy[7-9] is very useful for analyzing complicated molecular spectra. This method uses two independent lasers. A circularly polarized pump beam (dye laser 1, power of 100 mW) is fixed to a center of Doppler-free line of a known transition $B\,^1\Pi(v'=0,J')$–$X\,^1\Sigma^+(v''=4,J'')$, and is modulated by a chopper. A linearly polarized probe beam (dye laser 2; Coherent CR699-29, linewidth 500 kHz, Rhodamine 6G dye, power of 10 mW), which passes a linear polarizer P1, is propagated in the opposite direction to the pump beam through the heat pipe. When the probe laser is tuned, the polarization is altered if the frequency of the probe laser coincides with a center of the Doppler profile of transition lines which share a common level with the pump transition. Then, the probe beam passes the crossed linear polarizer P2 and reaches a photomultiplier PM2 (Hamamatsu R712). The signal output was detected by a lock-in amplifier 2 (EG&G model 5210). In order to confirm that the pump

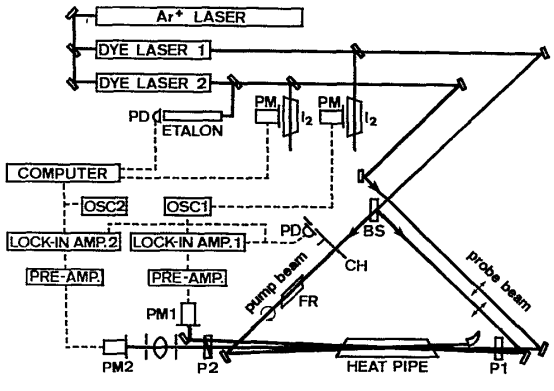

FIG. 2. Experimental setup for OODR polarization spectroscopy. BS: beam splitter, CH: chopper, FR: $\lambda/4$ Fresnel rhomb, P1 and P2: linear polarizers, PM1 and PM2: photomultipliers, OSC1 and OSC2: oscilloscopes, and PD: photodiode.

laser stayed on the center frequency of a selected transition, the signal of normal Doppler-free polarization spectrum was monitored during the measurement of a Doppler-free OODR polarization spectrum. Thus, the OODR polarization spectrum can be obtained without either Doppler broadening or Doppler shift. With a circularly polarized pump beam, only P and R transitions are detected, and the signs are different. If we use the pump beam polarized linearly at 45° to the probe polarization, only the Q transitions are detected. In a case where a large number of lines are overlapped, the Doppler-free OODR polarization spectroscopy is very useful to detect selectively a series of transitions from a chosen level. Due to its high sensitivity, very weak absorption lines can be detected.

NaK vapor was produced by heating a 1:4 mixture of sodium and potassium in a stainless steel heat pipe. The heat pipe oven was operated at 550 K with Ar as buffer gas of 0.4 Torr. The absolute wave numbers of the observed spectral lines were calibrated by the fluorescence excitation spectrum of iodine, and the fringe patterns of a confocal etalon (FSR = 150 MHz) were used as a frequency marker. The linewidth of the spectral line was sensitive to the vapor pressure and the laser power.

III. RESULTS AND DISCUSSION

A. Spectroscopic analysis

For a $^1\Pi$–$^1\Sigma^+$ transition, there are three branches, P, Q, and R. With a circularly polarized pump beam, only P and R transitions are detected in the OODR polarization spectrum, and the signs are different in P and R transitions. Hence, the assignments are easy and can be accurate. We chose the $B\,^1\Pi(v'=0,J'=18)$–$X\,^1\Sigma^+(v''=4,J''=17)$ transition at 16 476.1728 cm^{-1} as the pump transition, and the probe laser was scanned from 17 250 to 17 755 cm^{-1}. A part of the OODR polarization spectrum and the normal polarization spectrum of the $B\,^1\Pi(v',J'=16$ and $18)$–$X\,^1\Sigma^+(v''=4,J''=17)$ transitions are shown in Fig. 3, and the observed lines are listed in Table I.

In the normal polarization spectrum, the intensities of the transitions from the levels of $v''=0$ and 1 of the $X\,^1\Sigma^+$ state were strong, but the transitions from the $X\,^1\Sigma^+(v''=4,J''=17)$ level were not detected with appreciable intensity. In the OODR polarization spectrum, the P and R transitions from the selected $X\,^1\Sigma^+(v''=4,J''=17)$ level were observed predominantly. The extra lines of weak intensity are the transitions from the pumped $B\,^1\Pi(v'=0,J'=18)$ level and the collisionally depopulated $X\,^1\Sigma^+(v''=4,J'')$ levels.

The term energy is expressed in the form

$$E_{v,J}=E_v^0+B_v[J(J+1)-\Lambda^2]-D_v[J(J+1)-\Lambda^2]^2+\cdots, \quad (1)$$

where Λ is ± 1 for a $^1\Pi$ state and 0 for a $^1\Sigma^+$ state, B_v is the rotational constant, D_v is the centrifugal distortion constant, and E_v^0 is the energy of the vibrational state v:

$$E_v^0=T_e+G_v, \quad (2)$$

Downloaded from http://pubs.aip.org/aip/jcp/article-pdf/94/12/7713/8232721/7713_1_online.pdf

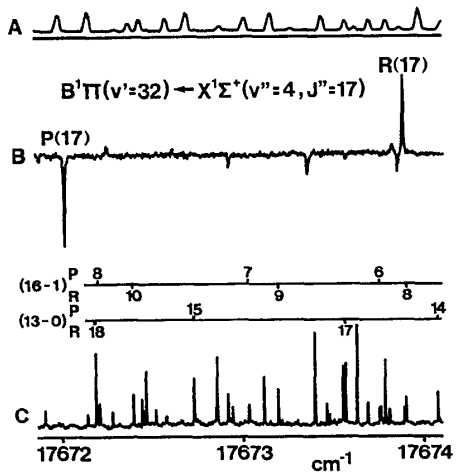

FIG. 3. Top (A) is the fluorescence excitation spectrum of I_2 for calibration of the absolute wave number. The second (B) is a part of the OODR polarization spectrum, where the $B\,^1\Pi(v'=0,\ J'=18)$–$X\,^1\Sigma^+(v''=4,\ J''=17)$ transition is used as the pump transition. Bottom (C) is the normal polarization spectrum and a part of the assignments.

TABLE I. Observed lines (in units of cm^{-1}) of the $^{23}Na^{39}K$ $B\,^1\Pi(v',\ J'=16$ and 18)–$X\,^1\Sigma^+(v''=4, J''=17)$ transitions measured by the OODR polarization spectroscopy. Pump beam is fixed to the $B\,^1\Pi(v'=0, J'=18)$–$X\,^1\Sigma^+(v''=4, J''=17)$ transition at 16 476.1728 cm^{-1}.

	Probe transitions	
v'	$B\,^1\Pi(v',16)$–$X\,^1\Sigma^+(4,17)$	$B\,^1\Pi(v',18)$–$X\,^1\Sigma^+(4,17)$
15	17 262.1180	17 265.6801
16	17 298.1477	17 301.5988
17	a	a
18	17 365.5094	17 368.7598
19	17 396.5714	17 399.7272
20	17 426.0677	17 429.1222
21	17 454.0121	17 456.9759
22	17 480.4105	17 483.2287
23	17 505.7997	17 508.4941
24	17 529.2262	17 531.8889
25	17 551.4083	17 553.9799
26	a	a
27	17 591.7914	17 594.2435
28	17 610.4232	17 612.6948
29	17 627.5589	17 629.7409
30	17 643.6550	17 645.7304
31	17 658.3327	17 660.0983
32	17 672.0339	17 673.8876
33	17 684.2674	17 686.0351
34	17 695.0490	17 696.6299
35	17 705.0780	17 706.5818
36	17 713.3327	17 714.7392
37	17 720.1784	17 721.4058
38	17 726.1100	17 727.1912
39	17 730.9772	17 731.9473
40	17 734.5880	17 735.4286
41	17 737.2491	17 737.9418
42	17 739.0423	17 739.5765
43	17 740.0896	17 740.4112

[a] Unlisted ones are strongly perturbed lines or weak and undetected lines.

where T_e is the minimum energy of the corresponding potential energy curve, and G_v is the vibrational energy. The energy separation between the $R(J)$ and $P(J)$ lines is given by

$$E_{v,J+1} - E_{v,J-1} = (4J+2)B_v - 2(J^2+J+1)(4J+2)D_v + \cdots. \quad (3)$$

For $J = 17$, the higher order terms can be neglected, but the terms up to D_v cannot be neglected.

At first, we have approximated the value of D_v by

$$D_v = \sum_{i=0,\ldots,3} Y_{i2}(v+1/2)^i, \quad (4)$$

where the Dunham coefficients Y_{i2} were determined for $v' = 0$–16 in Ref. 5. From a pair of $P(17)$ and $R(17)$ lines, which are listed in Table I, we calculated the values of B_v and E_v^0 for $v' = 15$–43. The values for $v' = 15$ and 16 were in good agreement with the values reported in Ref. 5. The E_v^0 and B_v values for $v' = 16$–43 and the values for $v' = 0$–15 in Ref. 5 were taken together as input data of least-squares fitting, which yielded the Dunham coefficients Y_{ij} ($j = 0$ and 1):[10]

$$E_v^0 - T_e - B_v = \sum_{i=0,\ldots,9} Y_{i0}(v+1/2)^i, \quad (5)$$

TABLE II. Molecular constants E_v^0 and B_v for $v' = 16$–43 of the $^{23}Na^{39}K$ $B\,^1\Pi$ state. All values are in units of cm^{-1}. The values for $v' = 0$–16 are given in Table I of Ref. 5.

v'	E_v^0	$10^2 B_v$
16	17 861.1958	4.987 02
17	...	...
18	17 929.3469	4.670 80
19	17 960.7753	4.535 57
20	17 990.6638	4.390 81
21	18 018.9592	4.261 33
22	18 045.9211	4.053 44
23	18 071.7892	3.876 87
24	18 095.3378	3.831 96
25	18 117.8719	3.702 33
26	...	...
27	18 158.7149	3.533 40
28	18 178.0436	3.276 82
29	18 195.5239	3.150 32
30	18 212.0298	2.999 98
31	18 227.9033	2.559 77[a]
32	18 241.2582	2.689 09
33	18 253.8189	2.570 06
34	18 265.3165	2.307 95
35	18 275.6352	2.203 69
36	18 284.2559	2.071 80
37	18 291.7836	1.824 06
38	18 298.2670	1.624 04
39	18 303.5555	1.471 17
40	18 307.6503	1.297 71
41	18 310.8655	1.098 69
42	18 313.2527	0.885 30
43	18 315.1014	0.596 02

[a] The anomalous value may be originating from the perturbation.

Downloaded from http://pubs.aip.org/aip/jcp/article-pdf/94/12/7713/9732731/7713_1_online.pdf

TABLE III. Dunham coefficients for the $B\,^1\Pi$ state of $^{23}Na^{39}K$. All values are in units of cm^{-1}. The value of T_e, Y_{i0} ($i = 0$ to 4), Y_{i1} ($i = 0$ to 3), and Y_{i2} ($i = 0$ and 1) were fixed to the values derived in Ref. 5.

T_e	16 992.744 6	Y_{01}	$7.238\,53\times10^{-2}$
Y_{00}	− 0.043 0	Y_{11}	$-1.177\,99\times10^{-3}$
Y_{10}	71.463 0	Y_{21}	$-1.350\,2\times10^{-5}$
Y_{20}	− 1.150 92	Y_{31}	$-4.793\,3\times10^{-7}$
Y_{30}	$-1.061\,3\times10^{-2}$	Y_{41}	$4.829\,77\times10^{-8}$
Y_{40}	$9.995\,0\times10^{-4}$	Y_{51}	$-6.886\,06\times10^{-10}$
Y_{50}	$-1.426\,56\times10^{-5}$	Y_{61}	$-1.139\,84\times10^{-11}$
Y_{60}	$-8.677\,83\times10^{-7}$	Y_{71}	$2.095\,34\times10^{-13}$
Y_{70}	$4.749\,96\times10^{-8}$	Y_{02}	$-2.898\,59\times10^{-7}$
Y_{80}	$-9.307\,86\times10^{-10}$	Y_{12}	$-1.939\,01\times10^{-8}$
Y_{90}	$6.673\,43\times10^{-12}$	Y_{22}	$6.453\,99\times10^{-10}$
		Y_{32}	$-7.753\,55\times10^{-12}$
		Y_{42}	$9.918\,47\times10^{-13}$
		Y_{52}	$-3.463\,51\times10^{-14}$

$$B_v = \sum_{i=0,\ldots,7} Y_{i1}\,(v + 1/2)^i, \tag{6}$$

where the values of T_e, Y_{i0} ($i = 0$–4), and Y_{i1} ($i = 0$–3) were fixed to those in Ref. 5. From the Dunham coefficients Y_{i0} and Y_{i1} obtained above, the rotationless potential curve of the $B\,^1\Pi$ state is constructed up to the $v' = 43$ level by the Rydberg–Klein–Rees (RKR) method.[11,12] We noticed that the inner wall of the RKR potential increases at $v' \geqslant 40$. We made a correction, and the method is described in the next section. For the corrected RKR potential curve, the values of E_v^0, B_v, and D_v are calculated by a computational method described by Hutson.[13] The obtained value of D_v was slightly different from the value of D_v approximated by Eq. (4). Hence, by using the new D_v value, we have calculated again the E_v^0 and B_v values from a pair of $P(17)$ and $R(17)$ lines in Table I, and the results are listed in Table II. From the new E_v^0 and B_v values for $v' = 16$–43 and those for $v' = 0$–15 in Ref. 5, we have calculated the Dunham coefficients, and the results are listed in Table III.

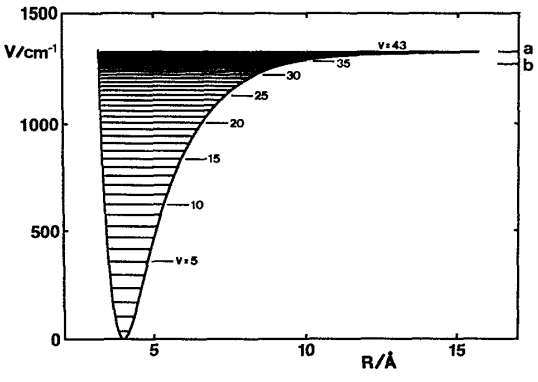

FIG. 4. The rotationless RKR potential energy curve of the NaK $B\,^1\Pi$ state. The horizontal lines show the observed vibrational levels. The dissociation limit to $Na(3s^2S_{1/2}) + K(4p^2P_{3/2})$ atoms is shown as a. The dissociation limit to $Na(3s^2S_{1/2}) + K(4p^2P_{1/2})$ atoms is shown as b.

TABLE IV. RKR-extrapolated potential of the $B\,^1\Pi$ state of $^{23}Na^{39}K$. R_- and R_+ are, respectively, inner and outer turning points of each vibrational level v. R_e is the equilibrium internuclear distance.

v	$V(R)/cm^{-1}$	R_-/Å	R_+/Å
		$R_e = 4.0134$ Å	
− 0.25	17.7507	3.8929	4.1489
0.	35.3995	3.8467	4.2103
1.00	104.5311	3.7402	4.3790
2.00	171.2929	3.6735	4.5105
3.00	235.6649	3.6229	4.6286
4.00	297.6453	3.5818	4.7402
5.00	357.2477	3.5470	4.8686
6.00	414.4992	3.5168	4.9556
7.00	469.4370	3.4903	5.0623
8.00	522.1065	3.4668	5.1696
9.00	572.5591	3.4457	5.2779
10.00	620.8503	3.4267	5.3879
11.00	667.0383	3.4095	5.4997
12.00	711.1827	3.3940	5.6138
13.00	753.3433	3.3798	5.7305
14.00	793.5799	3.3669	5.8499
15.00	831.9514	3.3551	5.9723
16.00	868.5156	3.3443	6.0981
17.00	903.3294	3.3344	6.2273
18.00	936.4479	3.3252	6.3603
19.00	967.9254	3.3168	6.4974
20.00	997.8143	3.3091	6.6388
21.00	1026.1658	3.3019	6.7849
22.00	1053.0292	3.2953	6.9360
23.00	1078.4516	3.2892	7.0926
24.00	1102.4776	3.2836	7.2552
25.00	1125.1485	3.2785	7.4243
26.00	1146.5016	3.2739	7.6007
27.00	1166.5694	3.2699	7.7854
28.00	1185.3787	3.2663	7.9795
29.00	1202.9500	3.2633	8.1846
30.00	1219.2966	3.2608	8.4026
31.00	1234.4244	3.2589	8.6361
32.00	1248.3322	3.2574	8.8885
33.00	1261.0122	3.2563	9.1642
34.00	1272.4524	3.2552	9.4689
35.00	1282.6387	3.2542	9.8107
36.00	1291.5601	3.2533	10.2008
37.00	1299.2149	3.2526	10.6542
38.00	1305.6190	3.2520	11.1919
39.00	1310.8181	3.2514	11.8416
40.00	1314.9014	3.2510	12.6368
41.00	1318.0209	3.2507	13.6009
42.00	1320.4140	3.2505	14.6841
43.00	1322.4316	3.2503	15.6318

B. Long-range potential of the $B\,^1\Pi$ state

From the Dunham coefficients Y_{i0} and Y_{i1}, the rotationless potential curve of the $B\,^1\Pi$ state was constructed up to $v' = 43$ by the RKR method.[11,12] Let us denote the outer and inner turning points of a vibrational level v as $R_+(v)$ and $R_-(v)$, respectively. The inner wall of the calculated RKR potential bent over at $v' \geqslant 40$ and the inner turning point $R_-(v')$ increased with v'. At $v' = 42$ and 43, the inner

Downloaded from http://pubs.aip.org/aip/jcp/article-pdf/94/12/7713/9732731/7713_1_online.pdf

wall increased abruptly. Such a nonphysical inner-wall behavior in the RKR inversion procedure was discussed by Wells, Smith, and Zare.[14] They showed that the RKR procedure was very sensitive to the errors in the B_v values, but relatively insensitive to the G_v values. The distance between the outer and inner classical turning points of a vibrational level v, $R_+(v) - R_-(v)$, is given by the Klein action integral f, which is calculated from the G_v values. We modified the inner wall by a repulsive potential:[15] $V(R) = A/R^{12} + B$, where R is the internuclear distance. The constants A and B were determined by fitting to the inner turning points of $v' = 30$ to 34; $A = 3.855\,47 \times 10^9\ \mathrm{cm}^{-1}\ \text{Å}^{12}$ and $B = -1450.79\ \mathrm{cm}^{-1}$ for the RKR potential calculated from the Dunham coefficients in Table III. The outer turning points were adjusted by adding the distance $R_+(v) - R_-(v)$ to the extrapolated inner turning points. The resulting RKR turning points are listed in Table IV, and are shown in Fig. 4.

Many theoretical studies on the long-range interactions of alkali metals[1,16-19] and the experimental studies by the crossed beam technique[20,21] have been reported. The long-range interaction energy between Na($3s$) and K($4p$) atoms may be expressed as[19]

$$V(R)^{\mathrm{int}} = -C_6/R^6 - C_8/R^8 - C_{10}/R^{10} - \cdots, \quad (7)$$

where C_6, C_8, and C_{10} are constants. These constants can be determined by analyzing outer RKR turning points in the long range.[22,23] According to the criterion proposed by LeRoy,[22] the inverse-power expansion of interaction energy is valid for $R \geqslant 2[(\langle r_A^2\rangle)^{1/2} + (\langle r_B^2\rangle)^{1/2}]$, where $\langle r_X^2\rangle$ is the expectation value of the square of the radius of the outermost electrons on atom X. For Na($3s$) + K($4s$), the value of $2[(\langle r_{\mathrm{Na}}^2\rangle)^{1/2} + (\langle r_{\mathrm{K}}^2\rangle)^{1/2}]$ is reported to be 10.8 Å.[6] The vibrational energy G_v is plotted against the $[R_+(v)]^{-6}$, and it is shown in Fig. 5. The plot is linear in the limit of large $R_+(v)$ and the constant C_6 is determined to be $37.4 \times 10^6\ \mathrm{cm}^{-1}\ \text{Å}^6$ from the slope. In the same way, we can determine the constant C_8 from a plot of $G_v - C_6/[R_+(v)]^6$ against $[R_+(v)]^{-8}$. However, an appreciable deviation from the linear fit in Fig. 5 is observed only at $[R_+(v)]^{-6} > 10^{-6}\ \text{Å}^{-6}$, where the inverse-power expansion of interaction energy becomes invalid. Hence, the interaction energy of higher order than the C_6/R^6 term is expected to be small at $R \geqslant 10$ Å and cannot be derived from the present data. Bussery and Aubert-Frécon[19] calculated the long-range coefficients by a perturbation model, and obtained $C_6 = 35.7 \times 10^6\ \mathrm{cm}^{-1}\ \text{Å}^6$ and $C_8 = -0.51 \times 10^8\ \mathrm{cm}^{-1}\ \text{Å}^8$. They neglected the effect of spin–orbit interaction (we shall discuss about this effect in the next section), but these values are in fairly good agreement with our results.

For long-range potentials expressed as

$$V(R) = D_e - C_n/R^n, \quad (8)$$

where D_e is the dissociation energy, LeRoy and Bernstein[24] derived the relation

$$\frac{dG_v}{dv} = K_n[D_e - G_v]^{(n+2)/2n}, \quad (9)$$

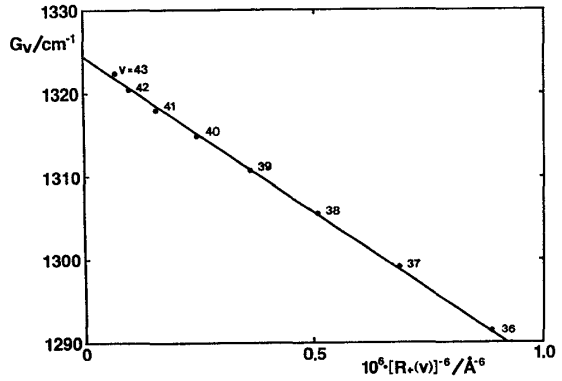

FIG. 5. Plots of G_v for high v levels in the $B\,^1\Pi$ state against $[R_+(v)]^{-6}$, where $R_+(v)$ is the outer turning point of a vibrational level v.

where K_n is a constant proportional to $C_n^{-1/n}$. For $n = 6$, it can be written as

$$(\Delta G_v)^{3/2} = (K_6)^{3/2}[D_e - G_v], \quad (10)$$

where $\Delta G_v = G_{v+1} - G_v$. The values of $(\Delta G_v)^{3/2}$ are plotted against G_v for the observed high v levels of the $B\,^1\Pi$ state in Fig. 6. The plot is linear and the dissociation energy is determined to be $1324.3 \pm 0.3\ \mathrm{cm}^{-1}$ from the extrapolation. The Birge–Sponer plot is shown in Fig. 7. Compared to the LeRoy–Bernstein plot (Fig. 6), there is more flexibility in extrapolating the convergence limit. The LeRoy–Bernstein plot is found to be more useful than the Birge–Sponer plot when transitions close to the dissociation limit, where the long-range potential can be expressed by Eq. (8), are observed.

Ross *et al.*[6] reported D_e of the $X\,^1\Sigma^+$ state to be $5274.9 \pm 0.5\ \mathrm{cm}^{-1}$. D_e of the $B\,^1\Pi$ state can also be obtained from the atomic energy level difference $\Delta E[\mathrm{K}(4p^2P_{3/2}) - \mathrm{K}(4s^2S_{1/2})] = 13\,042.89\ \mathrm{cm}^{-1}$ and the minimum electronic energy $T_e = 16\,992.7446\ \mathrm{cm}^{-1}$ reported in Ref. 5;

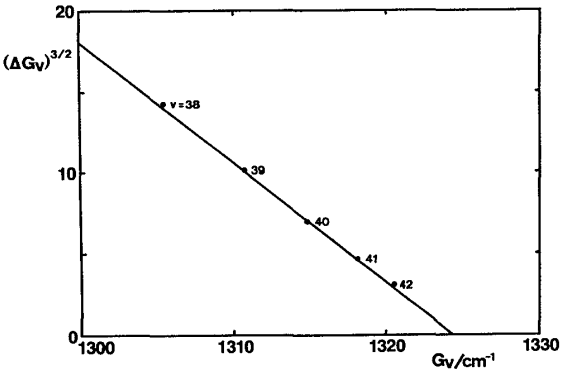

FIG. 6. LeRoy–Bernstein plot; $(\Delta G_v)^{3/2}$ is plotted against the vibrational term value G_v for high v levels in the $B\,^1\Pi$ state. The intercept of extrapolated line yields the dissociation energy $D_e = 1324.3 \pm 0.3\ \mathrm{cm}^{-1}$.

Downloaded from http://pubs.aip.org/aip/jcp/article-pdf/94/12/7713/9732731/7713_1_online.pdf

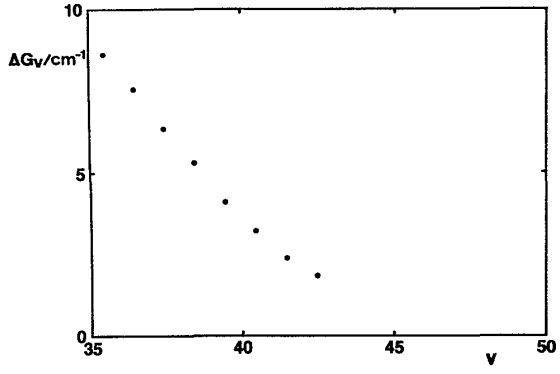

FIG. 7. Birge–Sponer plot; ΔG_v is plotted against v.

$$D_e(B\,^1\Pi) = D_e(X\,^1\Sigma^+) + \Delta E\,[\mathrm{K}(4p^2P_{3/2}) - \mathrm{K}(4s^2S_{1/2})] - T_e$$
$$= 1325.05 \pm 0.5\ \mathrm{cm}^{-1}.$$

This value and the one obtained by the LeRoy–Bernstein plot are coincident within the experimental errors.

C. Predissociation

The spectral line shapes of the $B\,^1\Pi(v' = 29$–43, $J' = 16)$–$X\,^1\Sigma^+(v'' = 4, J'' = 17)$ transitions are shown in Fig. 8. Similar spectral lines with opposite sign were observed for the R lines. A remarkable line broadening was observed for transitions to the levels of $v' \geqslant 33$. The energy threshold of the broadening is coincident with the dissocia-

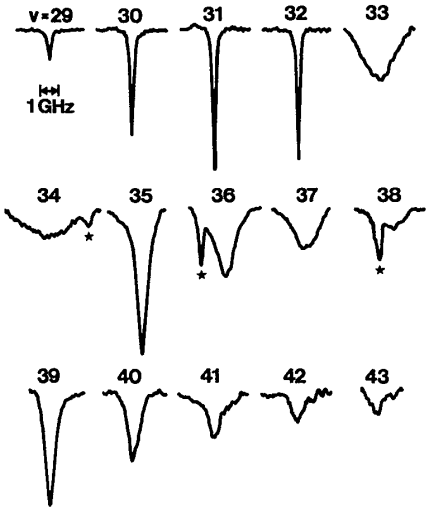

FIG. 8. The observed line shapes of the $B\,^1\Pi(v' = 29$–43, $J' = 16)$–$X\,^1\Sigma^+(v'' = 4, J'' = 17)$ transitions. The frequency scale is shown on the top. Lines with * are accidentally overlapped lines, which are not observed for the corresponding R lines.

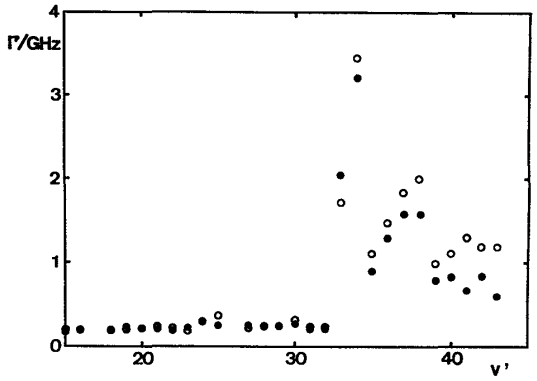

FIG. 9. The linewidths Γ of the $B\,^1\Pi(v' = 15$–43, $J' = 16$ and $18)$–$X\,^1\Sigma^+(v'' = 4, J'' = 17)$ transitions. An open circle (○) is for the R branch and a filled circle (●) for the P branch.

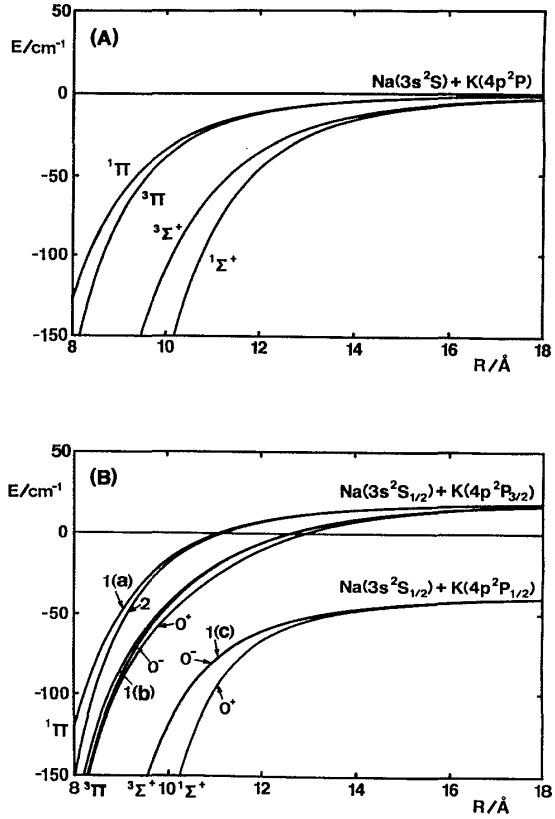

FIG. 10. Potential energy curves of NaK corresponding asymptote $Na(3s) + K(4p)$. (A): Spin–orbit interaction is neglected. The C_{10} values for $^1\Pi$, $^3\Pi$, $^1\Sigma^+$, and $^3\Sigma^+$ states are, respectively, -0.5, 4.3, 48, and -18 cm^{-1} Å^{10}. (B): Spin–orbit interaction is included. The numbers are the values of Ω in Hund's case (c) notation, and a letter in ( ) is a symbol to distinguish each.

Downloaded from http://pubs.aip.org/aip/jcp/article-pdf/94/12/7713/9732731/7713_1_online.pdf

tion limit to $Na(3s^2S_{1/2}) + K(4p^2P_{1/2})$ atoms, which is located 57.72 cm^{-1} below the one to $Na(3s^2S_{1/2}) + K(4p^2P_{3/2})$ atoms. Any irregular line shifts were not observed for all the broadened lines. The v' dependence of the linewidths (FWHM) of the $P(17)$ and $R(17)$ lines are plotted in Fig. 9. For the levels of $v' \leqslant 32$, the linewidth is observed to be about 200 MHz. However, the linewidth of $v' = 34$ is found to be 3.4 GHz. This line broadening may originate from the predissociation, and the rate can be estimated from the linewidth to be about $2 \times 10^{10}\ s^{-1}$ for $v' = 34$. The linewidth decreases somewhat for $v' \geqslant 35$, but is still broader than those for $v' \leqslant 32$.

In the Hund's case (a) representation there are four molecular states, $^1\Sigma^+$, $^1\Pi$, $^3\Sigma^+$, and $^3\Pi$, correlated with the separated atoms $Na(3s) + K(4p)$. By neglecting the spin–orbit interaction, Stevens *et al.*[25] calculated the potential energy curves for all these states up to $R = 20\ a_0$ by the full-valence configuration interaction computations. We added a $-C_{10}/R^{10}$ term to the long-range potential curve obtained by Bussery and Aubert–Frécon,[19] and the C_{10} value was determined so as to fit with the potential energies at $R = 15$ and $20\ a_0$ obtained by Stevens *et al.*[25] The resulting potential curves are shown in Fig. 10(A).

At long internuclear distances, the effect of the spin–orbit interaction cannot be neglected, and the electronic states transform into Hund's case (c) states. The $B\,^1\Pi(\Omega = \pm 1)$ state transforms into the 1(a) state at long internuclear distances, and the outer RKR turning points in the long-range determined above compose the potential curve of the 1(a) state. The energies and eigenfunctions for a given value of R can be obtained by diagonalizing the energy matrix composed of long-range interaction and spin–orbit interaction. The resulting energies are plotted in Fig. 10(B). The spin–orbit interaction mixes the $^1\Pi(\Omega = \pm 1)$, $^3\Pi(\Omega = \pm 1)$, and $^3\Sigma^+(\Omega = \pm 1)$ states, but the mixing of the $^3\Sigma^+(\Omega = \pm 1)$ state, which is correlated with the separated atoms $Na(3s^2S_{1/2}) + K(4p^2P_{1/2})$, is small for the 1(a) state (see Table V). The potential curve of the 1(a) state does not cross with any curves of the other states in the long range [see Fig. 10(B)]. Hence, the predissociation of the $B\,^1\Pi(\Omega = \pm 1)$ state to $Na(3s^2S_{1/2}) + K(4p^2P_{1/2})$ atoms through the interaction at long range is expected to be negligibly small.

In order to cause an appreciable predissociation, a repulsive potential curve must either come very near to, or cross, the $B\,^1\Pi$ state curve. According to the computations by Stevens *et al.*,[25] the $(2)^3\Sigma^+$ curve comes close to the $B\,^1\Pi$ curve on the inner limb and crosses just above the dissociation limit. The perturbation between the $B\,^1\Pi$ and $(2)^3\Sigma^+$ states can occur through the spin–orbit interaction H_{so}. The nonvanishing matrix elements are[26] $\langle B\,^1\Pi(v'J)|H_{so}|(2)^3\Sigma^+[vN(=J \text{ and } J \pm 1)J]\rangle$. The rate of the predissociation is approximately proportional to the product of the Franck–Condon factor $|\langle v'|v\rangle|^2$ and the electronic–rotational factor $|\langle B\,^1\Pi(J)|H_{so}|(2)^3\Sigma^+[N(=J \text{ and } J \pm 1)J]\rangle|^2$. From the variation of the linewidth with v' (see Fig. 9), the $(2)^3\Sigma^+$ potential curve probably crosses the $B\,^1\Pi$ curve near the left turning point of the $B\,^1\Pi(v' = 34)$ level. For such a crossing, we can expect on Franck–Condon considerations a very rapid rise of the predissociation just before the crossing and a gradual falling off at higher v'. We conclude that the remarkable line broadenings at $v' \geqslant 33$ occur through the predissociation to $Na(3s^2S_{1/2}) + K(4p^2P_{1/2})$ atoms, the predissociation is caused by a strong spin–orbit interaction between the $B\,^1\Pi$ and $(2)^3\Sigma^+$ states, and the potential curves cross around the inner turning point of the $B\,^1\Pi(v' = 34)$ level.

TABLE V. Eigenfunctions of 1(a, b, and c) states correlated with the separated atoms $Na(3s) + K(4p)$, which are expressed as a linear combination of the Hund's case (a) wave functions: $C_1|^3\Sigma^+_{\pm 1}\rangle + C_2|^1\Pi_{\pm 1}\rangle + C_3|^3\Pi_{\pm 1}\rangle$.

State	R/Å	Energy/cm^{-1}	C_1	C_2	C_3
1(a)	10	−17.657	0.023	0.760	−0.650
	10.5	−8.141	0.019	0.742	−0.670
	11	−1.371	0.016	0.731	−0.682
	11.5	3.520	0.013	0.724	−0.689
	12	7.105	0.011	0.720	−0.694
	13	11.772	0.008	0.714	−0.700
	14	14.469	0.006	0.712	−0.702
	16	17.107	0.004	0.709	−0.705
	18	18.190	0.002	0.708	−0.706
	20	18.682	0.002	0.708	−0.706
1(b)	10	−45.203	0.383	0.594	0.708
	10.5	−32.089	0.475	0.583	0.660
	11	−21.666	0.557	0.560	0.614
	11.5	−13.314	0.623	0.533	0.572
	12	−6.657	0.673	0.508	0.538
	13	2.745	0.735	0.471	0.489
	14	8.547	0.767	0.447	0.460
	16	14.437	0.796	0.423	0.431
	18	16.890	0.807	0.415	0.420
	20	18.002	0.812	0.412	0.415
1(c)	10	−121.842	0.923	−0.265	−0.278
	10.5	−97.139	0.880	−0.330	−0.341
	11	−80.463	0.831	−0.389	−0.399
	11.5	−69.136	0.782	−0.437	−0.444
	12	−61.319	0.740	−0.473	−0.478
	13	−51.844	0.679	−0.518	−0.521
	14	−46.750	0.641	−0.542	−0.543
	16	−42.047	0.605	−0.563	−0.563
	18	−40.203	0.591	−0.571	−0.571
	20	−39.384	0.584	−0.574	−0.574

ACKNOWLEDGMENT

H.K. and M.B. thank the ministry of education, science, and culture of Japan for a Grand-in-aid for Scientific Research.

[1] R. S. Mulliken, Phys. Rev. **120**, 1674 (1960).
[2] G. K. Chawla, H. J. Vedder, and R. W. Field, J. Chem. Phys. **86**, 3082 (1987).
[3] J. Heinze and F. Engelke, J. Chem. Phys. **89**, 42 (1988).
[4] R. F. Barrow, R. M. Clements, J. Derouard, N. Sadeghi, C. Effantin, J. d'Incan, and A. J. Ross, Can. J. Phys. **65**, 1154 (1987).
[5] H. Katô, M. Sakano, N. Yoshie, M. Baba, and K. Ishikawa, J. Chem. Phys. **93**, 2228 (1990).
[6] A. J. Ross, C. Effantin, J. d'Incan, and R. F. Barrow, Mol. Phys. **56**, 903 (1985).

Downloaded from http://pubs.aip.org/aip/jcp/article-pdf/94/12/7713/8732731/7713_1_online.pdf

[7] C. Wieman and T. W. Hänsch, Phys. Rev. Lett. **36**, 1170 (1976).
[8] R. E. Teets, F. V. Kowalski, W. T. Hill, N. Carlson, and T. W. Hänsch, SPIE, Vol. 113 Laser Spectroscopy (1977), p. 80.
[9] M. Raab, G. Höning, W. Demtröder, and C. R. Vidal, J. Chem. Phys. **76**, 4370 (1982).
[10] J. L. Dunham, Phys. Rev. **41**, 721 (1932).
[11] R. Rydberg, Z. Phys. **73**, 376 (1931); O. Klein, *ibid.* **76**, 226 (1932); A. L. G. Rees, Proc. Phys. Soc. London Ser. A **59**, 998 (1947).
[12] R. N. Zare, J. Chem. Phys. **40**, 1934 (1964).
[13] J. M. Hutson, J. Phys. B **14**, 851 (1981).
[14] B. H. Wells, E. B. Smith, and R. N. Zare, Chem. Phys. Lett. **99**, 244 (1983).
[15] R. J. LeRoy, J. Chem. Phys. **52**, 2683 (1970).
[16] G. W. King and J. H. Van Vleck, Phys. Rev. **55**, 1165 (1939).
[17] P. R. Fontana, Phys. Rev. **123**, 1865, 1871 (1961).
[18] A. Dalgarno and W. D. Davison, Mol. Phys. **13**, 479 (1967).
[19] B. Bussery and M. Aubert-Frécon, J. Phys. B **18**, L379 (1985).
[20] R. Düren, W. Gröger, and R. Liedtke, Chem. Phys. Lett. **109**, 424 (1984).
[21] L. Brencher, B. Nawracala, and H. Pauly, Z. Phys. D **10**, 211 (1988).
[22] R. J. LeRoy, *Molecular Spectroscopy*, (The Chemical Society, London, 1973), Vol. 1, p. 113.
[23] W. C. Stwalley, Chem. Phys. Lett. **7**, 600 (1970).
[24] R. J. LeRoy and R. B. Bernstein, J. Chem. Phys. **52**, 3869 (1970).
[25] W. J. Stevens, D. D. Konowalow, and L. B. Ratcliff, J. Chem. Phys. **80**, 1215 (1984).
[26] M. Baba, T. Nakahori, T. Iida, and H. Katô, J. Chem. Phys. **93**, 4637 (1990).

Downloaded from http://pubs.aip.org/aip/jcp/article-pdf/94/12/7713/8732731/7713_1_online.pdf